

# Oxygen Excess in $\text{La}_2\text{CoO}_{4+\delta}$ : A Neutron Diffraction Study

Ainara Aguadero<sup>a</sup>, José Antonio Alonso<sup>b</sup>, and Loreto Daza<sup>a</sup>

<sup>a</sup> Centro de Investigaciones Energéticas Mediambientales y Tecnológicas (CIEMAT),  
Av. Complutense 22, 28040 Madrid, Spain

<sup>b</sup> Instituto de Ciencia de Materiales de Madrid, CSIC, Cantoblanco, E-28049 Madrid, Spain

Reprint requests to Dr. A. Aguadero. E-mail: aguadero@ciemat.es

*Z. Naturforsch.* **2008**, *63b*, 615–622; received February 20, 2008

*Dedicated to Professor Gérard Demazeau on the occasion of his 65<sup>th</sup> birthday*

The layered perovskite  $\text{La}_2\text{CoO}_{4+\delta}$  has been prepared and characterized in order to identify its capability of incorporating interstitial oxygen atoms ( $\delta$ ) and their effect on the crystal structure. The synthesis has been performed by a citrate-nitrate soft-chemistry technique; a high oxygen pressure treatment (350 °C, 200 bar) has allowed us to increment the interstitial oxygen contents up to  $\delta = 0.32(1)$ . The samples have been characterized by thermal analysis (TG and DTA), X-ray diffraction at room temperature and neutron diffraction at temperatures up to 600 °C. At r. t., the as-prepared phase,  $\text{La}_2\text{CoO}_{4.22(1)}$ , is orthorhombic, space group *Bmab*, with an important orthorhombic strain, if compared with  $\text{La}_2\text{NiO}_{4+\delta}$ . At high temperatures it undergoes two consecutive structural transitions, to an orthorhombic superstructure at 375 °C and finally to a tetragonal symmetry (space group *F4/mmm*) at 590 °C. The phase  $\text{La}_2\text{CoO}_{4.32(1)}$  seems to represent a superstructure with orthorhombic symmetry and with a doubled *b* unit-cell parameter with respect to the prepared sample.

**Key words:**  $\text{K}_2\text{NiF}_4$  Structure, Neutron Diffraction, High Oxygen Pressure, Oxygen Stoichiometry, Cathode, SOFC

## Introduction

Recently, compounds with  $\text{K}_2\text{NiF}_4$  structure have attracted considerable attention due to their interesting transport properties that make them promising materials for several applications such as electrodes for solid oxide fuel cells (SOFC), catalysts and oxygen separation membranes [1–3].

The crystal structure of compounds with  $\text{K}_2\text{NiF}_4$  structure can be described as a stacking of perovskite layers,  $\text{ABO}_3$ , alternating with AO rock salt layers. The ionic conductivity mechanism of these materials is not clear yet, but it has been associated with the excess interstitial oxygen ( $\delta$ ) accommodated in the AO layers [4–6]. Previous work with  $\text{La}_2\text{NiO}_{4+\delta}$  demonstrated the suitability of these layered perovskites  $\text{A}_2\text{BO}_4$  as cathode materials for SOFCs [7]. In this regard, the introduction at the *B* position of the perovskite of a cation with a higher tendency than Ni to form the oxidation state *M*(III) would increase the interstitial oxygen content and therefore, improve the transport properties of these materials.

In this work we have analyzed the ability of  $\text{La}_2\text{CoO}_{4+\delta}$  to incorporate an excess of oxygen as an

interstitial defect. As-grown samples of  $\text{La}_2\text{CoO}_{4+\delta}$ , which are spontaneously oxidized in air under the synthetic conditions, were additionally subjected to heat treatments at moderate temperatures under high oxygen pressure. The effect of this treatment has been studied by X-ray and neutron diffraction as well as by thermal analysis.

## Experimental Section

The synthesis of  $\text{La}_2\text{CoO}_{4+\delta}$  has been performed via the nitrate-citrate route. Stoichiometric amounts of analytical grade  $\text{La}_2\text{O}_3$  and  $\text{Co}(\text{NO}_3)_2 \cdot 6\text{H}_2\text{O}$  (Panreac) were dissolved in 8 M  $\text{HNO}_3$  (Merck). Citric acid was then added to the mixture in a molar ratio 3.3 : 1 with respect to  $\text{La}_2\text{CoO}_{4+\delta}$ . The resulting product was dehydrated before being calcined at 600 °C for 30 min in air. The obtained precursors were annealed at 1200 °C for 12 h under  $\text{N}_2$  atmosphere to avoid the formation of unwanted Ruddlesden-Popper phases containing  $\text{Co}^{3+}$ , giving rise to a pure  $\text{La}_2\text{CoO}_{4+\delta}$  phase. Subsequent heat treatment under high oxygen pressure was performed at 350 °C and 200 bar of oxygen during 12 h in a VAS furnace. As-prepared and  $\text{O}_2$ -treated samples were characterized by X-ray diffraction (XRD) for phase identification and to assess phase purity. XRD analyses were performed with

a Philips X Pert-MPD diffractometer using  $\text{CuK}\alpha$  radiation ( $\lambda = 1.5406 \text{ \AA}$ ).

The cationic ratios were determined by inductively coupled plasma-atomic emission spectroscopy (ICP-AES) using a Jobin Yvon equipment. The oxygen content after and before the heat treatment was determined by thermogravimetric analysis between 25 and 900 °C in a  $\text{H}_2/\text{N}_2$  (5 % : 95 %) flow using a TG50 equipment. The stability in air was assessed by differential thermal analysis using a Stanton STA781 TG/DTA apparatus.

Neutron powder diffraction (NPD) data were collected at r. t. for the as-prepared and  $\text{O}_2$ -treated samples using the diffractometer D1A at ILL, Grenoble, France. The high intensity mode ( $\Delta d/d \geq 2 \times 10^{-3}$ ) was selected, with a neutron wavelength  $\lambda = 1.91 \text{ \AA}$  within the  $2\theta$  angular range from  $5^\circ$  to  $165^\circ$ . 3 g of each sample was contained in a vanadium can for the r. t. measurements whereas for the high-temperature measurements in air, the sample was placed in a quartz tube open to the ambient atmosphere and placed in the isothermal zone of a furnace with a vanadium resistor operating under vacuum ( $P_{\text{O}_2} \approx 10^{-6} \text{ Torr}$ ). The collection time was 2 h per pattern. Diffraction data were analyzed by Rietveld methods using the program FULLPROF [8]. The scattering lengths used were those incorporated in the program. The line shape of the diffraction peaks was generated by a pseudo-Voigt function and the background refined to a 5<sup>th</sup> degree polynomial. In the final run the following parameters were refined: background coefficients, zero point, half width, pseudo-Voigt and asymmetry parameters for the peak shape, scale factor and unit-cell parameters. Positional and occupancy factors for oxygen atoms and isotropic displacement factors were also refined for NPD data. The coherent scattering lengths for La, Co and O were 8.240, 2.49 and 5.803 fm, respectively.

In order to study the thermal expansion of  $\text{La}_2\text{CoO}_{4+\delta}$ , a dense sample was prepared pressing the powder into pellets (10 mm in diameter and 1.4 mm thickness) using polyethylene glycol as a binder and 3 tons of uniaxial pressure for 5 min. The pellet was then calcined at 1250 °C for 6 h under  $\text{N}_2$ . The thermal expansion of the dense ceramic was studied using a Linseis L75/1550C dilatometer with a heating rate of  $5 \text{ }^\circ\text{C} \cdot \text{min}^{-1}$ .

## Results and Discussion

ICP-AES data confirmed the cationic ratio to be as expected, excluding the presence of lanthanum or cobalt vacancies.

### Thermal analysis

The thermal stability of the materials in air was studied taking into account two aspects: The thermal evolution of the oxygen content in air was analyzed by

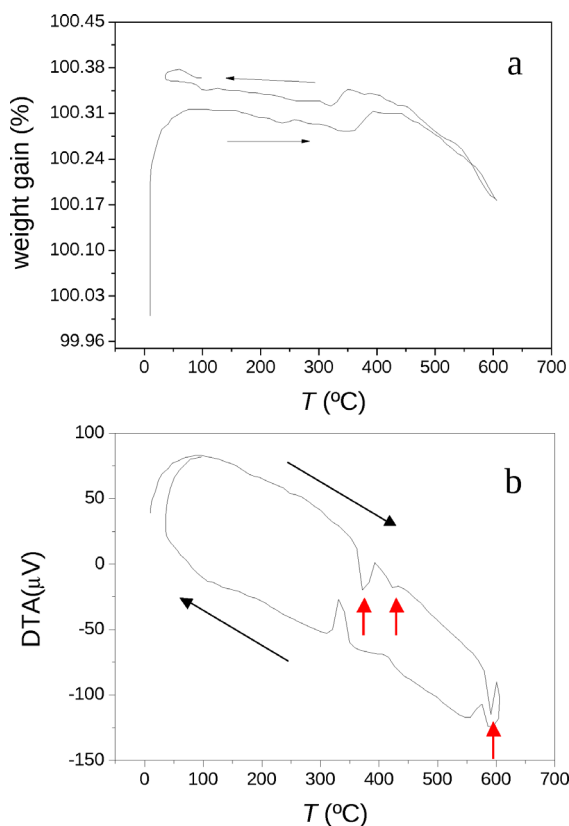


Fig. 1. Thermal analysis for the as-prepared  $\text{La}_2\text{CoO}_{4+\delta}$ : a) cycled TG and b) cycled DTA. Both of them are performed in air between 25–650 °C.

TG while the existence of phase transitions was determined by DTA.

The TG curves (Fig. 1a) of the prepared sample evidence a sizeable gain of weight of 0.32 % between 25 and 100 °C which is in accordance with the spontaneous oxidation of this compound described by other authors at r. t. [9, 10]. The sample is able to keep the oxygen content constant up to 450 °C after which it loses a small fraction ( $\sim 0.13 \%$ ) up to 600 °C. During the cooling step the sample recovers the lost oxygen mass finishing the experiment with an increase of 0.36 % of the total mass (0.08 mol of oxygen per formula unit) with respect to the beginning of the experiment. The DTA experiment under air (Fig. 1b) reveals the existence of three reversible processes. Upon heating, the three processes are endothermic and can be localized at 375, 420 and 590 °C, while upon cooling, they are exothermic at 332, 409 and 573 °C.

Other authors [11] have described two transitions at 387 and 577 °C instead of the three observed in our

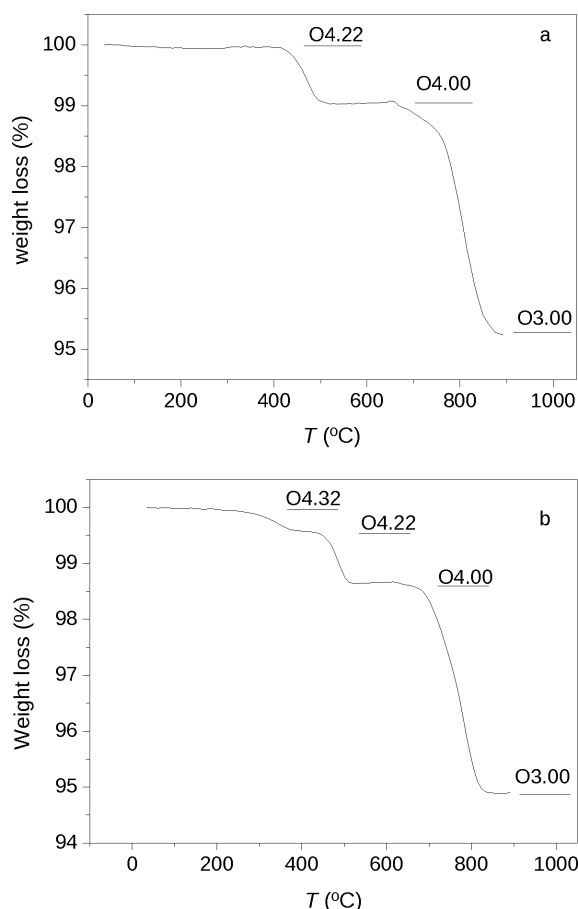


Fig. 2. TG curve under an  $\text{H}_2/\text{N}_2$  (5%:95%) flow between 25 and 1000 °C for a) the as-prepared sample and b) the oxygen-treated sample (350 °C, 200 bar).

case. The first one has been associated with a structural transition keeping orthorhombic symmetry, but having a direct influence on the physical properties of the system, since these authors detected an increase of the magnetic susceptibility and a reduction of the electrical resistance from this temperature on. The second transition has been attributed to a symmetry change from orthorhombic to tetragonal.

The oxygen gain of the sample between 100 and 400 °C has allowed us to establish that the optimal temperature for oxygen incorporation is 350 °C; for this reason the thermal treatment at high oxygen pressure was carried out at 350 °C, under 200 bar of  $\text{O}_2$  pressure.

The determination of the oxygen contents, before and after the  $\text{O}_2$  treatment, was also performed by thermal analysis under reducing conditions ( $\text{H}_2/\text{N}_2$  flow).

Fig. 2 shows the TG curves obtained. On the one hand, the huge ability of oxygen intake exhibited by this Co layered perovskite is remarkable, since the as-prepared sample already shows  $\delta > 0$  even though the synthesis process was carried out in  $\text{N}_2$  atmosphere. The as-prepared sample displays an oxygen stoichiometry  $\text{La}_2\text{CoO}_{4.22(1)}$ . On the other hand, it shows a great capacity to admit a still larger amount of interstitial oxygen after an additional treatment under high  $\text{O}_2$  pressure, giving rise to an increment of 0.1 mole of oxygen per formula unit as the  $\text{O}_2$ -treated sample has the stoichiometry  $\text{La}_2\text{CoO}_{4.32(1)}$ .

#### X-Ray diffraction

The X-ray diffraction (XRD) patterns of  $\text{La}_2\text{CoO}_{4+\delta}$  showed pure  $\text{K}_2\text{NiF}_4$  phases for both the as-prepared and the  $\text{O}_2$ -treated perovskites. Rietveld refinement of the crystal structures from XRD data proceeded satisfactorily in the orthorhombic space group  $Bmab$ . The atomic positions are specified in the next section. Fig. 3 shows the goodness of the fit for  $\text{La}_2\text{CoO}_{4.32(1)}$ . It is worth mentioning the greater orthorhombic distortion presented by the  $\text{O}_2$ -treated sample as indicated by the unit cell parameters for  $\text{La}_2\text{CoO}_{4.22(1)}$  ( $a = 5.4874(1)$ ,  $b = 5.5329(1)$ ,  $c = 12.5507(3)$  Å), as compared to  $\text{La}_2\text{CoO}_{4.32(1)}$  ( $a = 5.4433(1)$ ,  $b = 5.5513(1)$ ,  $c = 12.6159(3)$  Å). The significant expansion observed in the  $c$  axis is directly related to the incorporation of extra oxygen atoms in interstitial positions of the NaCl layer of this perovskite. The orthorhombic strain, defined as  $S =$

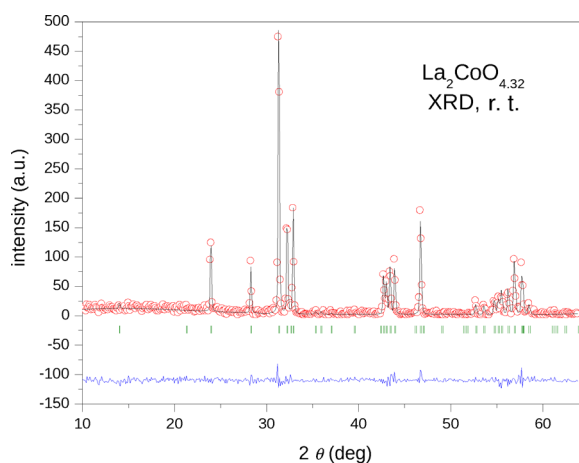


Fig. 3. Observed (points) and calculated (full curve) X-ray diffraction profile for oxygen-treated  $\text{La}_2\text{CoO}_{4+\delta}$  using a single-phase  $Bmab$  model.

$2(b-a)/(a+b)$ , is  $S = 8.25 \times 10^{-3}$  and  $9.82 \times 10^{-3}$  for the as-prepared and the  $\text{O}_2$ -treated samples, respectively; in both cases this value is much higher than that observed in  $\text{La}_2\text{NiO}_{4+\delta}$  of  $S = 1.23 \times 10^{-3}$  [12] which is probably ascribable to the much higher capacity to incorporate interstitial oxygen atoms of the Co-containing sample.

### Neutron diffraction

Room temperature neutron powder diffraction measurements have been performed for as-prepared and  $\text{O}_2$ -treated  $\text{La}_2\text{CoO}_{4+\delta}$ . The structure of the as-prepared material ( $\text{La}_2\text{CoO}_{4.22(1)}$ ) was refined by Rietveld methods as a single phase in the orthorhombic space group  $Bmab$  leading to a good fit between the calculated and the experimental data with  $R_{\text{Bragg}} = 5.7\%$  (Fig. 4). In the space group  $Bmab$ , La was located at  $8f$   $(0, y, z)$  positions, Ni at  $4a$   $(0, 0, 0)$  sites, and the four types of crystallographically independent oxygen atoms, O1 to O4, at  $8e$   $(1/4, 1/4, z)$ ,  $8f$   $(0, y, z)$ ,  $32m$   $(x, y, z)$  and  $16j$   $(1/4, 1/4, z)$ , respectively. The O4 site corresponds to interstitial oxygen atoms. The exact position of the interstitial oxygen atoms was determined by means of a difference Fourier map (Fig. 5), starting from a model without interstitials; the final position for these extra atoms is  $(0.2492, 0.2461, 0.2370)$  in equivalent sites.

However, the Rietveld fit of the NPD pattern for the  $\text{O}_2$ -treated phase ( $\text{La}_2\text{CoO}_{4.32(1)}$ ) in the space group  $Bmab$  was not totally satisfactory since there remained some unexplained extra diffraction peaks. A pattern

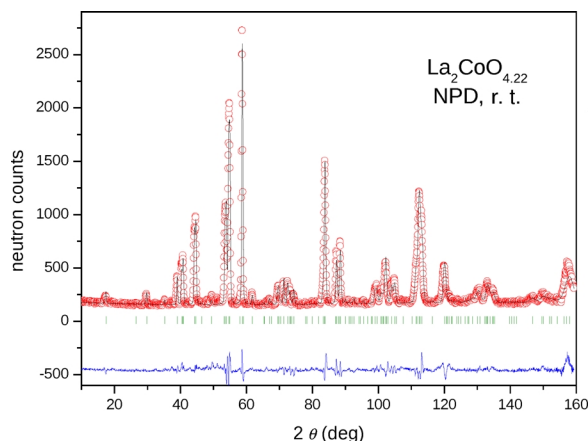


Fig. 4. Observed (points) and calculated (full curve) neutron diffraction profile for as-prepared  $\text{La}_2\text{CoO}_{4+\delta}$  using a single-phase  $Bmab$  model.

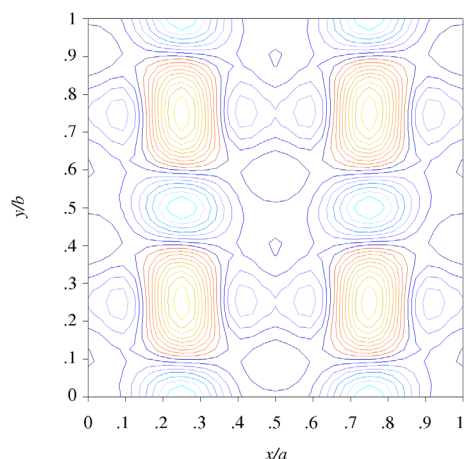


Fig. 5. Fourier map for the localization of interstitial oxygen atoms in  $\text{La}_2\text{CoO}_{4+\delta}$ .

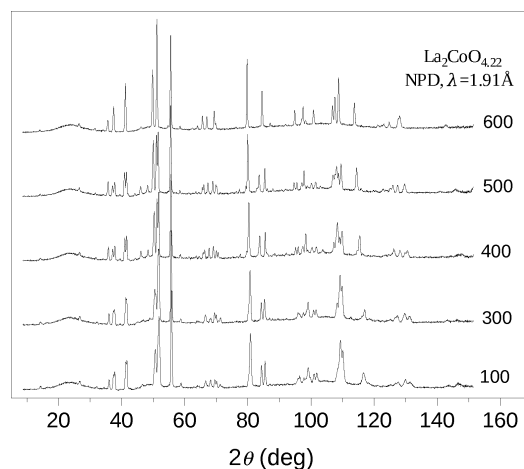


Fig. 6. Neutron powder diffraction patterns for  $\text{La}_2\text{CoO}_{4+\delta}$  collected at 100, 200, 300, 400, 500, and 600 °C.

matching (Le Bail fit) of the NPD data in a unit cell with a doubled  $b$  axis, in the space group  $Pmmm$ , led to an acceptable fit of the pattern, which suggests that there is a long-range ordering of the interstitial oxygen atoms giving rise to a superstructure along the  $b$  direction.

In parallel with the structural study at r. t., we carried out an investigation of the thermal evolution of the crystal structure in air of the as-prepared compound. If we compare the NPD diagrams obtained at different temperatures there is evidence for two structural transitions, one between 300 and 400 °C and a second one between 500 and 600 °C (Fig. 6). This is in agreement with the two endothermic peaks observed by means of DTA at 375 and 590 °C (Fig. 1b).

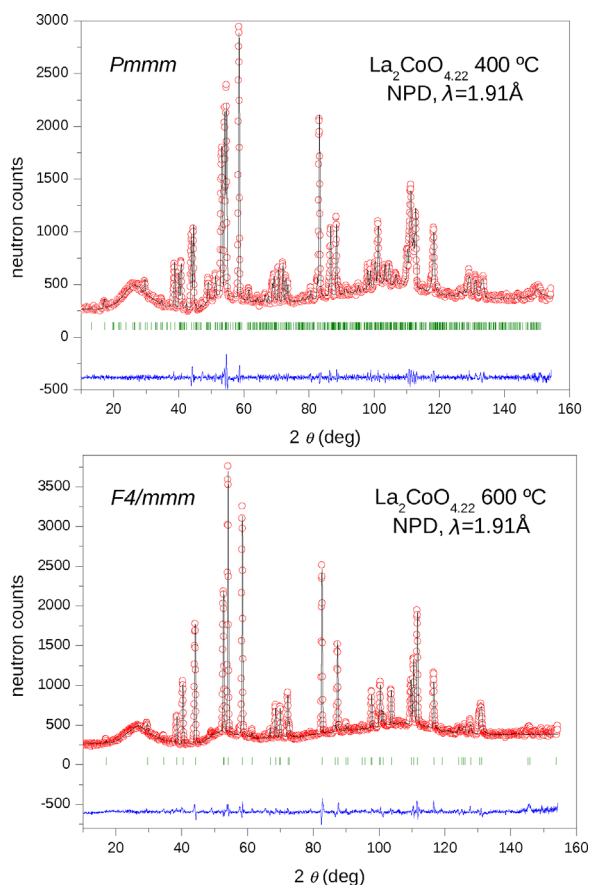


Fig. 7. Observed (points) and calculated (full curve) neutron diffraction profiles for a)  $\text{La}_2\text{CoO}_{4+\delta}$  at 400 °C using a pattern-matching fit in the space group  $Pmmm$ , where the  $b$  parameter has been doubled, and b)  $\text{La}_2\text{CoO}_{4+\delta}$  at 600 °C using a single-phase  $F4/mmm$  model.

At 375 °C, the observed endothermic effect has been associated with an orthorhombic-orthorhombic transition in the literature [11]. In our NPD data we observe the emergence of some extra peaks at 400 °C that could not be explained in the space group  $Bmab$ . A pattern matching with the same unit cell parameters in the space group  $Pmmm$ , lacking systematic extinctions, did not allow us to account for the extra reflections, clearly indicating the presence of a superstructure. A subsequent pattern matching with a doubled  $b$  axis was successful to explain all the reflections and satisfactorily fit the NPD pattern (Fig. 7a). These results suggest that we are again dealing with a superstructure along the  $b$  direction due to the long-range ordering of interstitial atoms, of the same nature as observed for the  $\text{O}_2$ -treated sample at r. t.

Table 1. Structural parameters of  $\text{La}_2\text{CoO}_{4+\delta}$  at r. t. (space group  $Bmab$ ) and 600 °C (space group  $F4/mmm$ )<sup>a</sup>.

	r. t.	600 °C
$a$ , Å	5.47813(3)	5.52745(9)
$b$ , Å	5.53399(2)	5.52745(9)
$c$ , Å	12.65714(6)	12.8814(3)
$V$ , Å <sup>3</sup>	383.712(3)	393.56(1)
La:		
$y$	-0.0035(9)	0
$z$	0.3609(1)	0.3578(1)
$B$ , Å <sup>2</sup>	0.75(3)	2.02(4)
$n$	1.0	1.0
Co:		
$B$ , Å <sup>2</sup>	0.83(9)	2.3(1)
$n(\text{Co})$	0.5	0.5
O1:		
$z$	-0.0076(3)	0
$B$ , Å <sup>2</sup>	0.95(4)	2.36(6)
$n$	1.0	1.0
O2:		
$y$	0.013(2)	0
$z$	0.1727(3)	0.171(1)
$B$ , Å <sup>2</sup>	1.2(1)	2.3(1)
$n$	0.703(1)	0.46(3)
O3:		
$x$	0.048(2)	-0.067(3)
$y$	-0.097(3)	-0.067(3)
$z$	0.182(1)	0.176(1)
$B$ , Å <sup>2</sup>	1.2(1)	2.3(1)
$n$	0.297(1)	0.54(3)
O4:		
$z$	0.2395(3)	0.25
$B$ , Å <sup>2</sup>	0.68(5)	4.1(6)
$n$	0.087(1)	0.154(7)
$\chi^2$	3.05	2.8
$R_p$ , %	3.69	3.24
$R_{wp}$ , %	4.65	4.24
$R_{exp}$ , %	2.70	2.67
$R_{Bragg}$ , %	5.71	5.05

<sup>a</sup>  $n$ : Chemical stoichiometry of each element.

The endothermic peak at 590 °C (Fig. 1b) can be associated with an orthorhombic-to-tetragonal transition, leading to the merging of several groups of diffraction peaks owing to the increase in symmetry. The crystal structure at 600 °C was correctly Rietveld-refined in the tetragonal space group  $F4/mmm$ , with La and O2 atoms located at  $8e$  (0, 0,  $z$ ) sites, Co at  $4a$  (0, 0, 0), O1 at  $8c$  ( $1/4$ ,  $1/4$ , 0), O3 at  $32m$  ( $x$ ,  $y$ ,  $z$ ) and the interstitial O4 atoms at  $16e$  ( $1/4$ ,  $1/4$ ,  $z$ ) positions, leading to a good reliability factor  $R_{Bragg} = 5\%$ . Fig. 7b displays the good agreement between the observed and calculated neutron profiles. It should be pointed out that the irregular background observed in Figs. 7a and 7b is due to the quartz container, which allowed us to acquire the NPD data in an air atmosphere.

For the sake of comparison, we also Rietveld-refined the structure between r. t. and 500 °C in the space group  $Bmab$  and at 600 °C in the tetragonal space group  $F4/mmm$ . Table 1 includes the structural parameters obtained for the r. t. and 600 °C samples. Fig. 8

Bond	r. t.	100 °C	300 °C	400 °C	500 °C	600 °C
La–O1 $\times 2^a$	2.683(4)	2.678(7)	2.580(7)	2.617(6)	2.643(6)	2.678(2)
La–O1 $\times 2$	2.568(4)	2.581(7)	2.694(7)	2.695(6)	2.691(6)	
La–O2*	2.385(4)	2.393(6)	2.46(3)	2.426(8)	2.402(8)	2.40(1)
La–O2 $\times 2^a$	2.7725(6)	2.77(2)	2.767(4)	2.765(1)	2.772(1)	2.789(1)
La–O2	2.709(9)	2.83(3)	2.65(3)	2.751(2)	2.78(1)	
La–O2	2.89(1)		2.93(3)	2.86(2)	2.85(1)	
La–O3 $\times 2$	2.34(1)	2.36(3)	2.357(5)	2.421(3)	2.435(3)	2.40(2)
La–O3 $\times 2$	3.09(1)	2.18(4)	3.036(4)	3.076(2)	2.536(2)	3.18(1)
La–O3 $\times 2$	2.61(1)	2.94(10)	2.571(4)	2.579(2)	2.240(6)	2.46(2)
La–O3 $\times 2$	2.32(2)	2.77(10)	2.48(1)	2.244(6)	3.128(2)	
La–O4 $\times 2$	2.489(4)	2.55(2)	2.468(7)	2.529(4)	2.493(4)	
La–O4 $\times 2$	2.316(3)	2.26(2)	2.326(7)	2.286(4)	2.322(4)	2.398(1)
Co–O1 $\times 4$	1.9494(2)	1.9483(3)	1.9513(3)	1.9541(3)	1.9561(3)	1.9542(0)
Co–O2 $\times 2$	2.187(4)	2.173(6)	2.10(3)	2.159(8)	2.201(8)	2.21(1)
Co–O3 $\times 4$	2.38(1)	2.39(3)	2.276(4)	2.336(2)	2.358(2)	2.33(2)

Table 2. Thermal evolution of the main interatomic distances of  $\text{La}_2\text{CoO}_{4+\delta}$ .

<sup>a</sup> For the tetragonal phase (600 °C) the multiplicity of this bond is 4.

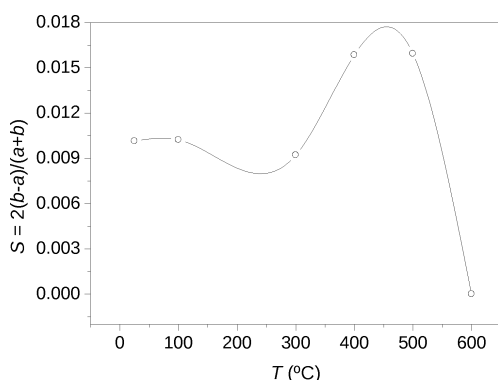


Fig. 8. Thermal evolution of the orthorhombic distortion ( $S$ ).

represents the variation of the orthorhombic strain with temperature; there is a great increase of the orthorhombic distortion when heating the sample up to 400 °C, whereupon it falls to  $S = 0$  upon the orthorhombic-to-tetragonal transition.

Table 2 includes the main bonding parameters for  $\text{La}_2\text{CoO}_{4+\delta}$ . The La–O1 bond lengths show a slight tendency to increase with temperature, exhibiting an average increase of 0.055 Å from r. t. to 600 °C. The shortest La–O2 distance, responsible for the cohesion between the perovskite and the rock-salt layer, increases with temperature up to 300 °C, and then it decreases in an opposite way with respect to those observed for the axial Co–O2 distances of the  $\text{CoO}_6$  octahedra. Thus, the compression along the  $c$  direction in the perovskite layer is accompanied by an expansion in the LaO rock-salt layer as a consequence of the incorporation of extra oxygen atoms, as it has been shown for  $\text{La}_2\text{NiO}_{4+\delta}$  before [12].

Equatorial Co–O1 bond lengths tend to increase with temperature. However a slight decrease is ob-

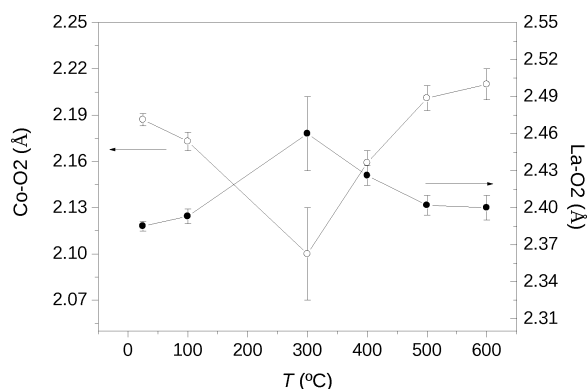


Fig. 9. Thermal evolution of Co–O2 and La–O2 bond lengths.

served at 100 and 600 °C, along with the concomitant behavior of the  $a$  and  $b$  unit cell parameters. Conversely, axial Co–O2 bond lengths decrease reaching a minimum value at 300 °C and then increase with temperature (Fig. 9). This shortening of the axial Co–O2 bond length is more pronounced than the connected La–O2 bond-length expansion, leading to an overall contraction of the cell at this temperature as it has been also observed by dilatometry analysis.

The thermal evolution of the oxygen content studied by neutron powder diffraction shows a similar behavior to that observed by means of thermogravimetric analysis (Fig. 1 a). Fig. 10 shows the temperature dependence of the oxygen excess ( $\delta$ ) obtained by the refinement of the occupancy factor of the interstitial positions, position O4. The oxygen stoichiometry tends to highly increase up to 500 °C and, then, slightly decreases at 600 °C. It is worth noting the high increase of the isotropic displacement factor for O4 from r. t. ( $0.68(5) \text{ \AA}^2$ ) to 600 °C ( $4.1(6) \text{ \AA}^2$ ) which may indicate

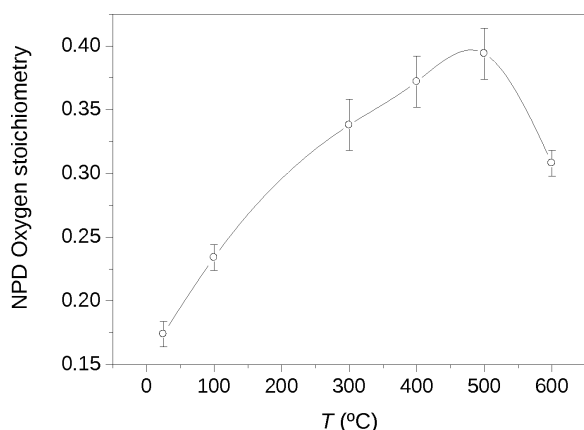


Fig. 10. Oxygen stoichiometry determined by neutron powder diffraction (NPD) as a function of temperature for  $\text{La}_2\text{CoO}_{4+\delta}$ .

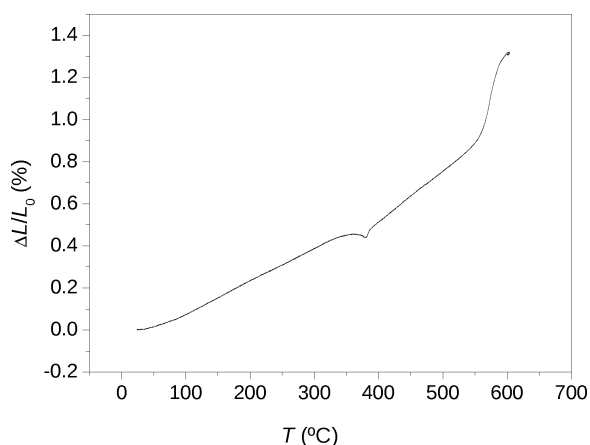


Fig. 11. Thermal expansion of  $\text{La}_2\text{CoO}_{4+\delta}$ .

a high mobility for the interstitial oxygen atoms in this compound.

#### Thermal expansion measurements

Thermal expansion measurements on a dense pellet between r.t. and 600 °C with a heating rate

of 5 °C · min<sup>-1</sup> show an abrupt contraction of  $\text{La}_2\text{CoO}_{4+\delta}$  at around 380 °C (Fig. 11). This contraction matches with the orthorhombic-orthorhombic phase transition observed by DTA at 375 °C (Fig. 1b) and could be related to the contraction observed in the Co–O2 bond length possibly induced by the huge oxygen gain that produced the expansion of the LaO layer and the concomitant contraction of the perovskite layer. The final increase of the thermal expansion is connected to the structural transition at 590 °C.

#### Conclusions

The compound  $\text{La}_2\text{CoO}_{4+\delta}$  has been successfully prepared *via* a nitrate-citrate route followed by annealing in a N<sub>2</sub> flow, with  $\delta = 0.22(1)$ . The subsequent thermal treatment under high oxygen pressure (300 °C, 200 bar) allowed us to increase the oxygen content up to  $\delta = 0.32(1)$ . The ability of this compound to absorb large amounts of oxygen upon slight heating in air is remarkable. The increase of interstitial oxygen atoms of about 0.1 mol per formula unit upon treatment under high O<sub>2</sub> pressure conditions seems to generate a superstructure due to the long-range ordering of the interstitial oxygen atoms along the *b* axis. The r. t. crystal structure for  $\text{La}_2\text{CoO}_{4.22}$  can be defined in the space group *Bmab*, showing a considerable orthorhombic strain due to the incorporation of extra oxygen atoms; when heating in air this sample undergoes two consecutive structural transitions, exhibiting at 600 °C a tetragonal structure containing elongated CoO<sub>6</sub> octahedra with large displacement factors for the interstitial oxygen atoms O4.

#### Acknowledgements

We thank for the financial support of CICYT to the project MAT2007-60536 and of the Madrid Community to the project ENERCAM-CM S-0505/ENE/0304. We thank the Institute Laue Langevin, Grenoble, France, for making all facilities available.

- [1] V. V. Kharton, A. P. Viskup, A. V. Kovalvsky, E. N. Naumovich, F. M. B. Marques, *Solid State Ionics* **2001**, *143*, 1174–1178.
- [2] Y. Wang, H. Nie, S. Wang, T. Wen, U. Guth, V. Valshook, *Mater. Lett.* **2006**, *60*, 26–37.
- [3] V. V. Kharton, A. A. Yaremchenko, A. L. Shaula, M. V. Patrekeev, E. N. Naumovich, D. I. Logvinovich, J. R. Frade, F. M. B. Marques, *J. Solid State Chem.* **2004**, *177*, 26–37.
- [4] E. N. Naumovich, M. V. Patrekeev, V. V. Kharton, A. A. Yaremchenko, D. I. Logvinovich, F. M. B. Marques, *Solid State Sci.* **2005**, *7*, 1353–1362.
- [5] V. V. Kharton, A. A. Yaremchenko, E. N. Naumovich, *J. Solid State Electrochem.* **1999**, *3*, 303–326.
- [6] L. Minervini, R. W. Grimes, J. A. Kilner, K. E. Sickafus, J. C. Grenier, Ph. Stevens, *J. Mater. Chem.* **2000**, *10*, 2349–2354.

- [7] A. Aguadero, M. J. Escudero, M. Pérez, J. A. Alonso, V. Pomjakushin, L. Daza, *Dalton Trans.* **2006**, 4377–4383.
- [8] J. Rodríguez-Carvajal, *Physica B* **1993**, 192, 55–69.
- [9] A. Nemudry, P. Rudolf, R. Schöllhorn, *Solid State Ionics* **1998**, 109, 213.
- [10] F. Girgsdies, R. Schöllhorn, *Solid State Chem.* **1994**, 91, 111.
- [11] P. Lehude, M. Daire, *C. R. Acad. Sci.* **1973**, 276, 1783.
- [12] A. Aguadero, J. A. Alonso, M. J. Martínez-Lope, M. T. Fernández-Díaz, M. J. Escudero, L. Daza, *J. Mater. Chem.* **2006**, 16, 3402–3408.